GROUND DATA PROCESSING & PRODUCTION OF THE LEVEL 1 HIGH RESOLUTION MAPS

VALERI 2001

Puéchabon site
(mediterranean forest)

Philippe Rossello

October 2007

CONTENTS

1. Introduction

This report describes the production of high resolution, level 1, biophysical variable maps for the Puéchabon site in 2001 (see campaign report for more details about the site and the ground measurement campaign: annex or http://www.avignon.inra.fr/valeri). Level 1 map corresponds to the map derived from the determination of a transfer function between reflectance values of the SPOT image acquired during (or around) the ground campaign, and biophysical variable measurements (hemispherical images). For each Elementary Sampling Unit (ESU), the hemispherical images were processed using the CAN-EYE software (Version 5) developed at INRA-CSE. The derived biophysical variable maps are:

• four Leaf Area Index (LAI) are considered: effective LAI (LAIeff) and true LAI (LAItrue) derived from the measurement of the gap fraction as a function of the view zenith angle; effective LAI57 (LAI57eff) and true LAI57 (LAI57true) derived from the gap fraction at 57.5°, which is independent on leaf inclination. Effective LAI and effective LAI57 do not take into account clumping effect. LAItrue and LAI57true are derived using the method proposed by Lang and Xiang[1] (1986);

• cover fraction (fCover): it is the percentage of soil covered by vegetation. To improve the spatial sampling, fCover was computed over 0 to 10° zenith angle;

• fAPAR: it is the fraction of Absorbed Photosynthetically Active Radiation (PAR = 400-700nm). fAPAR is defined either instantaneously (for a given solar position) or integrated all over the day. Following a study based on radiative transfer model simulations, it has been shown that the root mean square error between instantaneous fAPAR computed every 30 minutes and the daily fAPAR is the lowest for instantaneous fAPAR at 10h00 AM (solar time, RMSE = 0.021). Therefore, the derivation of fAPAR from CAN-EYE corresponds to the instantaneous black sky fAPAR at 10h00 AM.

The Puéchabon site corresponds to a “mediterranean forest mainly composed of oaks, box trees, and thyme”. This flat area is approximately 3 x 3 km with coordinates described in Table 1:

	UTM 31, North WGS-84 (units = meters)		Geographic Lat/Lon WGS-84 (units = degrees)	
	Easting	Northing	Lat.	Lon.
Upper left corner	550987.0000	4843010.0000	43.73837354	3.63317714
Lower right corner	554027.0000	4839970.0000	43.71078806	3.67062120
Center	552507.0000	4841490.0000	43.72458232	3.65190347

Table 1. Description of the site coordinates.

The ground measurements were carried out from 11th to 15th June 2001 and the high spatial resolution image (SPOT2, HRV2, resolution: 20 m) was acquired during the campaign.

2. Available data

2.1. SPOT Image

The SPOT image was acquired on 12th June 2001 by HRV2 on SPOT2. It was geo-located by SPOT image (SPOTView Basic product, level 2B). The projection is UTM 31, North, WGS-84. As the SPOT geo-location and the ground control points (GPS) were associated to some errors, a new geometric correction was performed by INRA. No atmospheric correction was applied to this image. However, as the SPOT image is used to compute empirical relationships between reflectance and biophysical variable, we can assume that the effect of the atmosphere is the same over the whole 3 x 3 km site. Therefore, it will be taken into account everywhere in the same way.

Figure 1 shows the relationship between Red and near infrared (NIR) SPOT channels: the soil line is marked and no saturated points are observed.

[1] Lang, A.R.G. and Xiang, Y., 1986. Estimation of leaf area index from transmission of direct sunlight in discontinuous canopies. Agric. For. Meteorol., 37: 229-243.

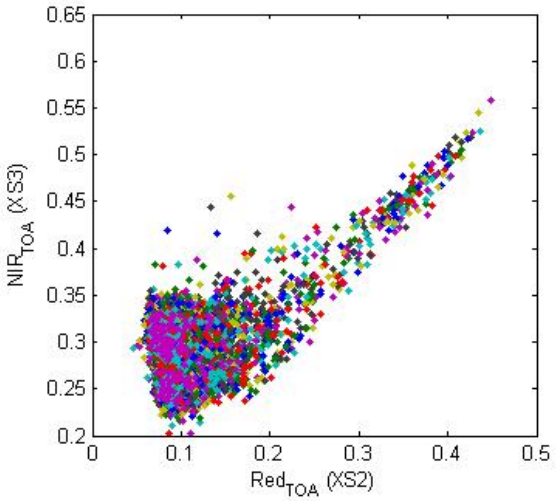

Figure 1. Red/NIR relationship on the SPOT image for Puéchabon, 2001.

2.2. Hemispherical images

The hemispherical images were processed using the CAN-EYE software (Version 5) to derive the biophysical variables. Figure 2 and Figure 3 show the distribution of the several variables over the 69 sampled ESUs. As Puéchabon site is mainly covered of a mediterranean forest, the hemispherical images were acquired from above the understorey and from below the canopy (trees). The two sets of acquisition were processed separately to derive LAI (effective and true), LAI57 (effective and true), fCover, and fAPAR. The ESU biophysical variable was then computed as:

- LAIeff, LAI57eff, LAItrue, LAI57true: LAI(above) + LAI(below).
- fCover: 1-(1-fCover(above))*(1-fCover(below)). This assumes independency between the gaps inside the understorey and those inside the trees which is not true at all the scales but it is the only way to get the total fCover. However, for the local scales considered, this might be true as a first order approximation.
- fAPAR: 1-(1-fAPAR(below))*(1-fAPAR(above)), since 1-fAPAR can be considered equivalent to a gap fraction. Here again, the same independency between the two layers has to be assumed.

However, if the understorey is not significant, the hemispherical images were only acquired from below the canopy and conversely, if the canopy is not significant, the hemispherical images were only acquired from above the understorey.

Note that LAI (effective and true) derived from directional gap fraction and LAI derived from gap fraction at 57.5° (effective and true) are consistent (Figure 2 and Figure 3). Effective LAI (LAIeff, LAI57eff) varies from 0.14 to 3.4, while true LAI (LAItrue, LAI57true) varies from 0.16 to 5.68. The site is thus heterogeneous in terms of LAI (Figure 2). LAIeff and LAI57eff are lower than LAItrue and LAI57true, due to the clumping observed for several ESUs. The relationship between fAPAR and LAI is in agreement with what is expected (Beer-Lambert law) while the fCover-LAI relationship is (slightly) more noisy (Figure 3).

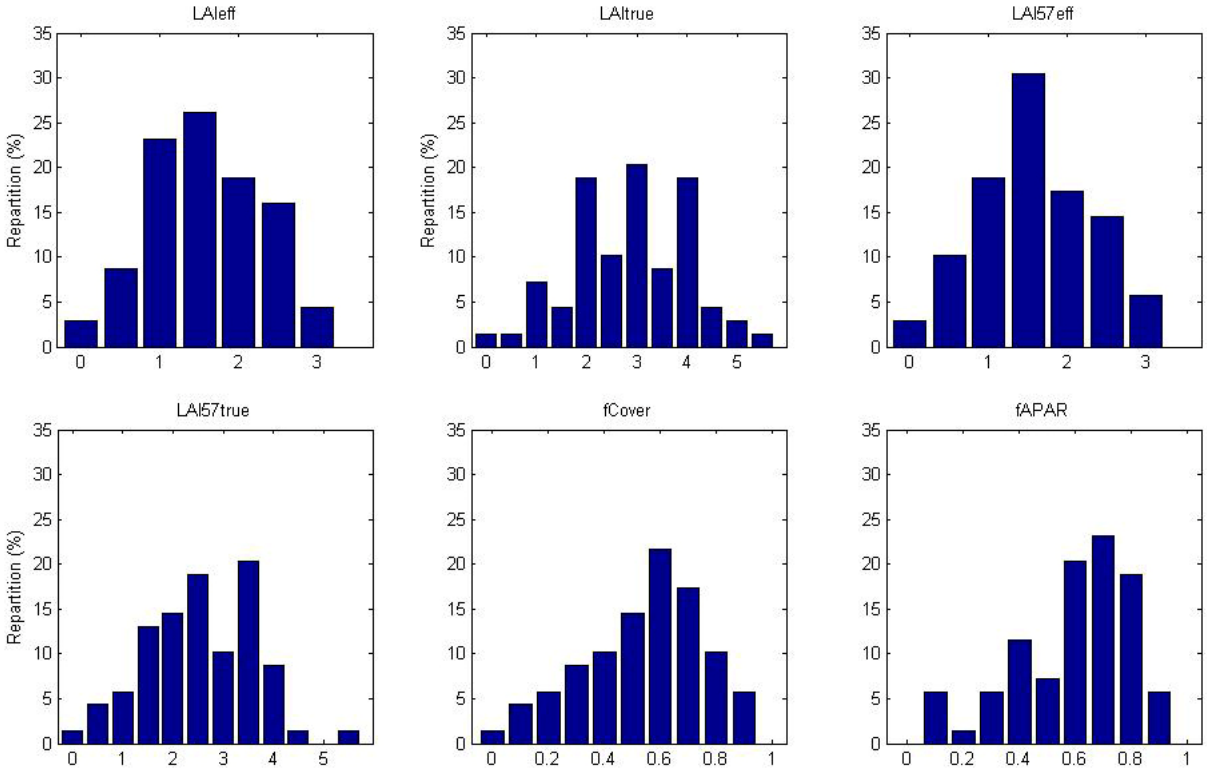

Figure 2. Distribution of the measured biophysical variables over the ESUs.

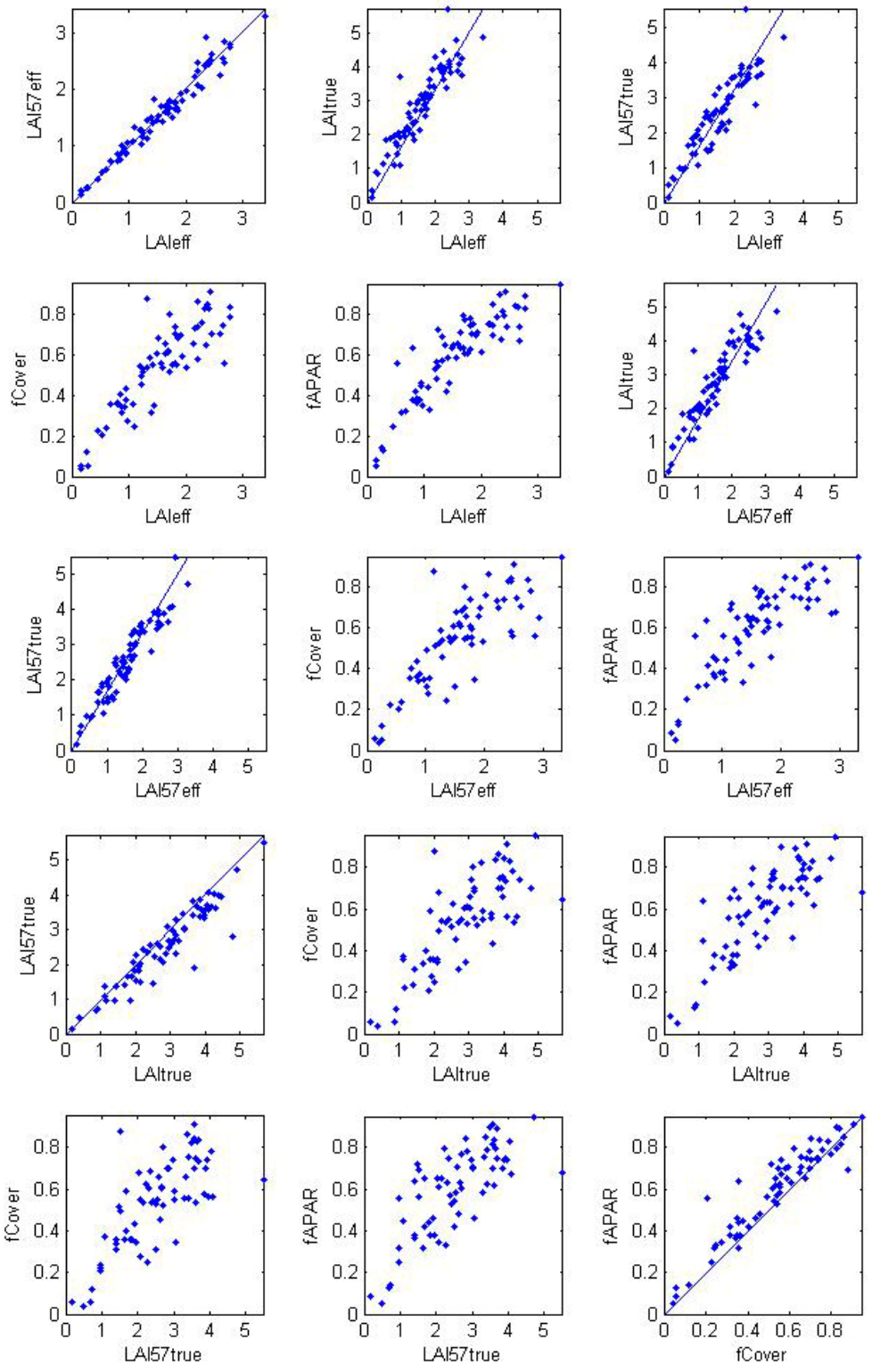

Figure 3. Relationships between the different biophysical variables.

2.3. Sampling strategy

2.3.1. Principles

The sampling strategy and measurement protocol are described in the campaign report (annex or http://www.avignon.inra.fr/valeri). Figure 4 shows that the 69 ESUs are evenly distributed over the site (3 x 3 km). The processing of the ground data has shown that:

- ESU E35 (in black on Figure 4) was located on a small plot with a strong heterogeneity on the borders. This ESU was eliminated;
- considering that SPOT geo-location and GPS measurements are associated to errors, we found that processed LAI for ESUs E1, E8, E9,E17, E38 and E39 did not correspond to the SPOT pixel in terms of reflectance as compared to the knowledge of the land use: they have been shifted by 1 or 2 pixels.

Finally, 68 ESUs have been kept for the computation of the transfer function.

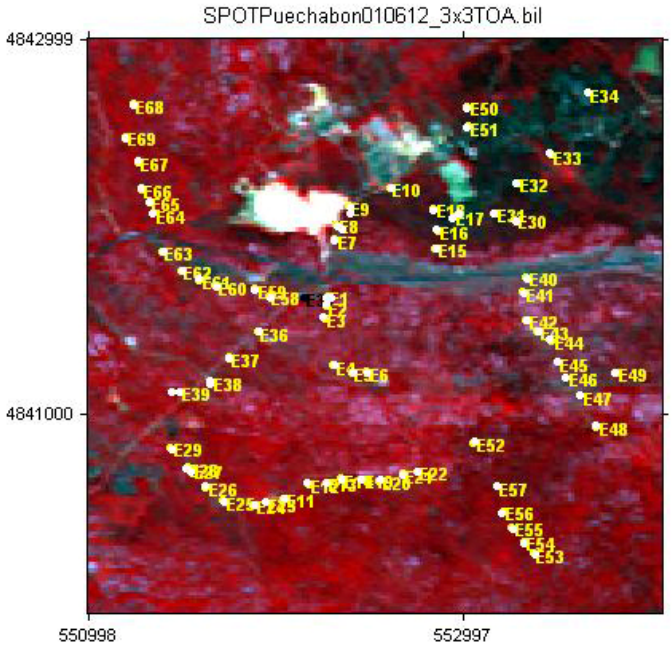

Figure 4. Distribution of the ESUs around the Puéchabon site.

2.3.2. Evaluation based on NDVI values

The sampling strategy is evaluated using the SPOT image by comparing the NDVI distribution over the site with the NDVI distribution over the ESUs (Figure 5). As the number of pixels is drastically different for the ESUs and whole site (WS = 22500 in case of a 3 x 3 km SPOT image, resolution 20m), it is not statistically consistent to directly compare the two NDVI histograms. Therefore, the proposed technique consists in comparing the NDVI cumulative frequency of the two distributions by a Monte-Carlo procedure which aims at comparing the actual frequency to randomly shifted sampling patterns. It consists in:

1. computing the cumulative frequency of the N pixel NDVI that correspond to the exact ESU locations;
2. then, applying a unique random translation to the sampling design (modulo the size of the image);
3. computing the cumulative frequency of NDVI on the randomly shifted sampling design;
4. repeating steps 2 and 3, 199 times with 199 different random translation vectors.

This provides a total population of $N = 199 + 1$(actual) cumulative frequency on which a statistical test at acceptance probability $1 - \alpha = 95\%$ is applied: for a given NDVI level, if the actual ESU density function is between two limits defined by the $N\alpha/2 = 5$ highest and lowest values of the 200 cumulative frequencies, the hypothesis assuming that WS and ESU NDVI distributions are equivalent is accepted, otherwise it is rejected.

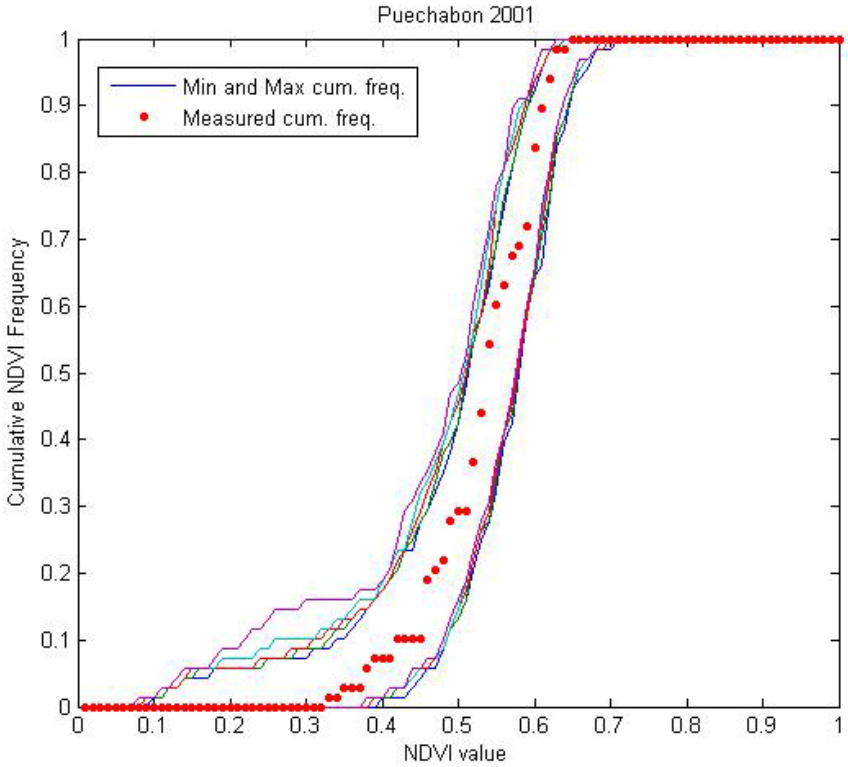

Figure 5. Comparison of the ESU NDVI distribution and the NDVI distribution over the whole image.

Figure 5 shows that the NDVI distribution of the 68 ESUs is very good over the whole site (comprised between the 5 highest and lowest cumulative frequencies). Note that NDVIs lower than 0.33 (roads, bare soil, rocks…) have not been sampled although they are present in the image.

2.3.3. Evaluation based on classification

A non supervised classification based on the k_means method (Matlab statistics toolbox) was applied to the 3 reflectances of the SPOT image to distinguish if different behaviours on the image for the biophysical variable-reflectance relationship exist.

A number of 4 classes was chosen (Figure 6). Except class 3, the distribution of the classes on the image and on the ESUs is comparable. Class 3 mainly corresponds to a quarry (LAI = 0).

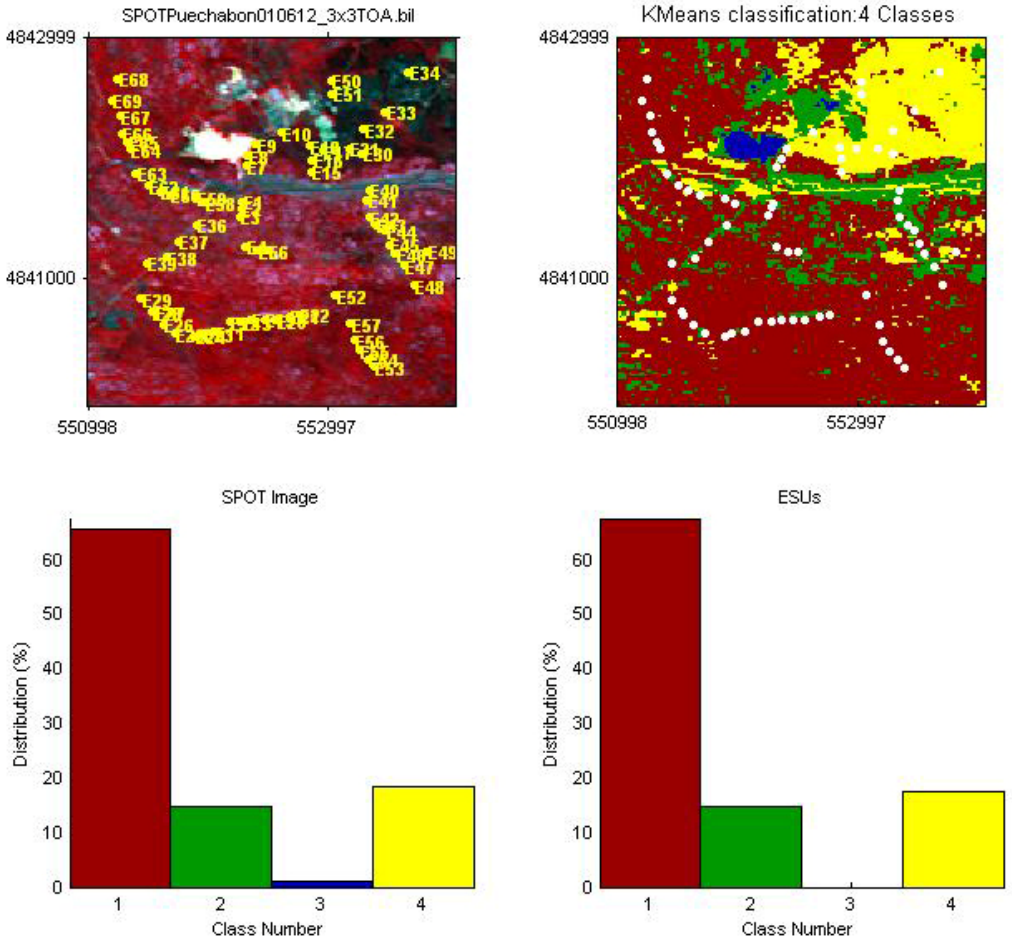

Figure 6. Classification of the SPOT image. Comparison of the class distribution between the SPOT image and sampled ESUs.

Figure 7 shows the different relationships observed between the biophysical variables and the corresponding NDVI on the ESUs, as a function of the SPOT classes determined from non supervised classification.

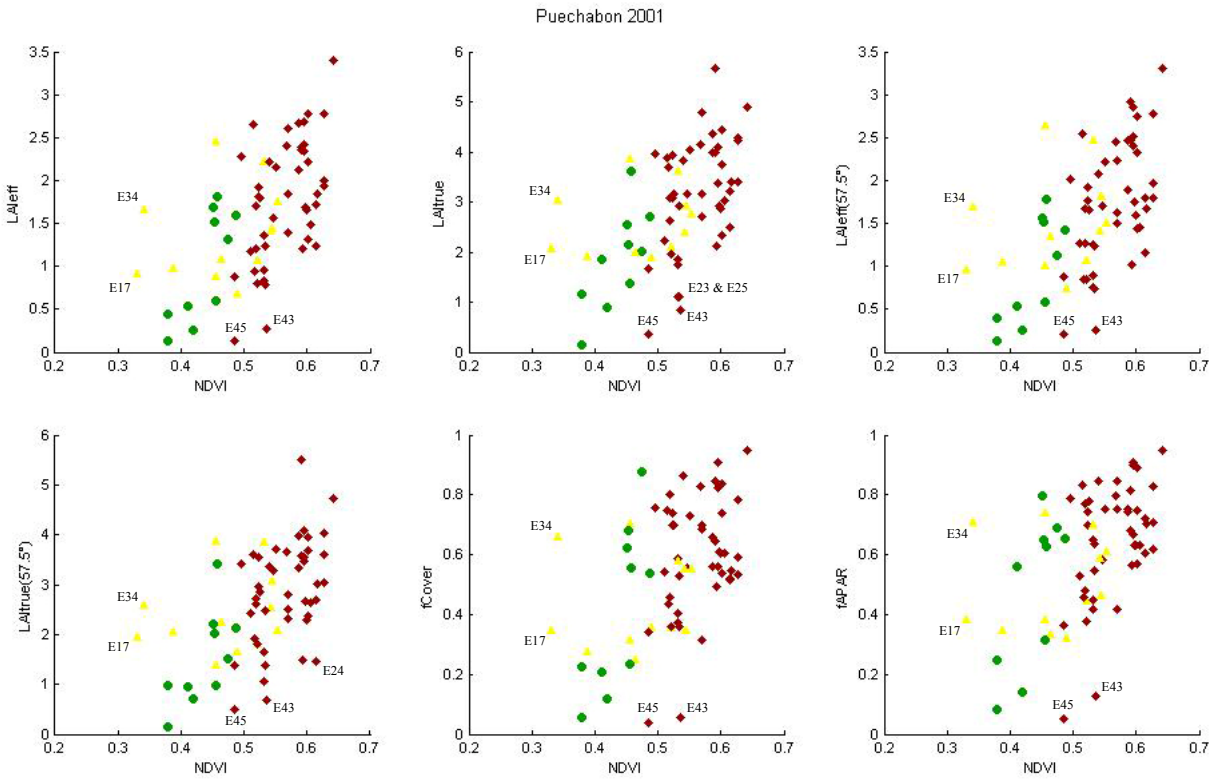

Figure 7. NDVI-Biophysical Variable relationships as a function of SPOT classes

The relation between NDVI and biophysical variables is consistent. Even if no different behaviour between the classes can be observed, some ESUs differ from the others (Figure 7): the biophysical variable values are relatively high while NDVIs are low (or conversely).

2.3.4. Using convex hulls

A test based on the convex hulls was also carried out to characterize the representativeness of ESUs. Whereas the evaluation based on NDVI values uses two bands (red and NIR), this test uses the three bands of the SPOT image. A flag image, is computing over the reflectances (Figure 8). The result on convex-hulls can be interpreted as:

- pixels inside the 'strict convex-hull': a convex-hull is computed using all the SPOT reflectance corresponding to the ESUs belonging to the class. These pixels are well represented by the ground sampling and therefore, when applying a transfer function the degree of confidence in the results will be quite high, since the transfer function will be used as an interpolator;
- pixels inside the 'large convex-hull': a convex-hull is computed using all the reflectance combination (±5% in relative value) corresponding to the ESUs. For these pixels, the degree of confidence in the obtained results will be quite good, since the transfer function is used as an extrapolator (but not far from interpolator);
- pixels outside the two convex-hulls: this means that for these pixels, the transfer function will behave as an extrapolator which makes the results less reliable. However, having a priori information on the site may help to evaluate the extrapolation capacities of the transfer function.

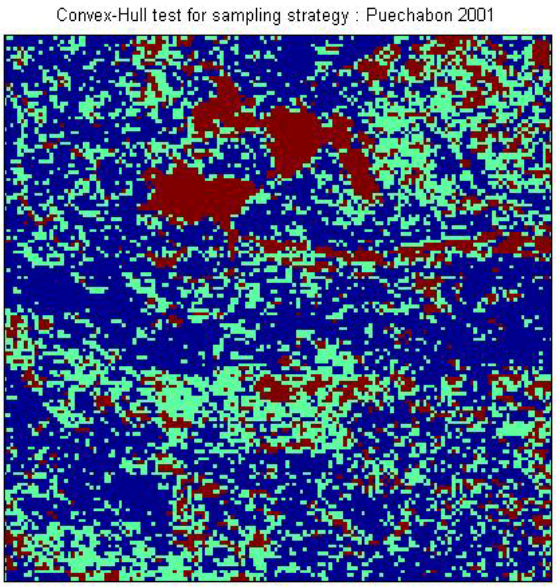

Figure 8. Evaluation of the sampling based on the convex hulls. The map is shown: blue and light blue correspond to the pixels belonging to the 'strict' and 'large' convex hulls and red to the pixels for which the transfer function is extrapolating.

This map shows that the representativeness of the ESUs is good, even if pixels are outside the two convex-hulls. They correspond to bare soil, rocks, NDVI pixels lower than 0.33 which have not been sampled (§2.3.2).

3. Determination of the transfer function for the 6 biophysical variables: LAIeff, LAItrue, LAI57eff, LAI57true, fCover, fAPAR

3.1. The transfer functions considered

Two types of transfer functions are usually tested in the frame of the VALERI project:

- AVE: if the number of ESUs belonging to the class is too low. The transfer function consists only in attributing the average value of the biophysical variable measured on the class to each pixel of the SPOT image belonging to the class;

- REG: if the number of ESUs is sufficient, multiple robust regression between ESUs reflectance (or Simple Ratio) and the considered biophysical variable can be applied: we used the 'robustfit' function from the matlab statistics toolbox. It uses an iteratively re-weighted least squares algorithm, with the weights at each iteration computed by applying the bisquare function to the residuals from the previous iteration. This algorithm provides lower weight to ESUs that do not fit well. The results are less sensitive to outliers in the data as compared with ordinary least squares regression. At the end of the processing, three errors are computed: classical root mean square error (RMSE), weighted RMSE (using the weights attributed to each ESU) and cross-validation RMSE (leave-one-out method).

The relationship between NDVI and LAI (§2.3.3) being consistent, the 'REG' method is applied to classes 1, 2 and 4. As class 3 corresponds to a quarry and no ESU belongs to this class, the value 0 is attributed to it.

The 'REG' function is tested using either the reflectance or the logarithm of the reflectance for any band combination as well as the simple ratio or NDVI. As the method has poor extrapolation capacities, a flag image, based on the convex hulls is computing over reflectances.

3.2. Results

3.2.1. Choice of the method

A single transfer function was thus computed for classes 1, 2 and 4. Figure 9 shows the results obtained for all the possible band combinations using either the reflectance (ρ) or the logarithm of the reflectance (log(ρ)).

Even if the regression made on the log(ρ) sometimes provides very slightly better results, the results using the reflectance (ρ) were selected for all the variables. The transfer function using the log(ρ) indeed creates coplanar points which do not allow the determination of the 'strict' and 'large' convex hulls.

Note that the Red*NIR ('+' or RN) combination is added to all the band combinations (except for NDVI and SR). Please read the document: "a method to improve the relation between the biophysical variables" (http://www.avignon.inra.fr/valeri/table_methods/new_linear.pdf).

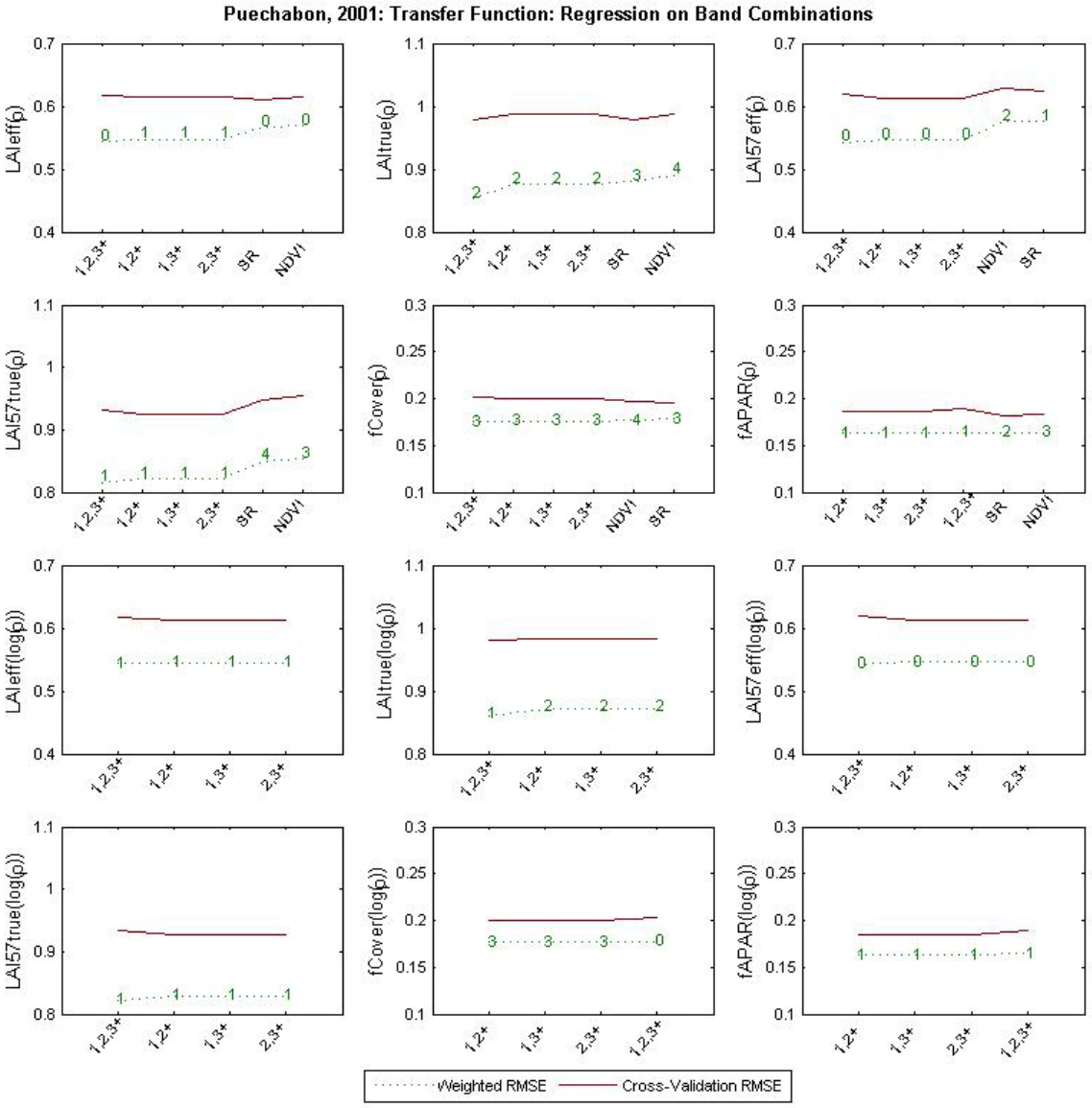

Figure 9. Transfer function: test of multiple regression applied on different band combinations. Band combinations are given in abscissa. The estimated biophysical variable is given in ordinate. Top graphs correspond to regression made on reflectance (ρ): the weighted root mean square error (RMSE) is presented in green along with the cross-validation RMSE in red. The numbers indicate the number of data used for the robust regression with a weight lower than 0.7 that could be considered as outliers. Bottom graphs correspond to regression made on the logarithm of the reflectance.

3.2.2. Choice of the band combination

For the LAIeff, the XS1, XS2, XS3, RN combination on reflectance (Figure 10 and Figure 11) was selected since it provides satisfactory results: weighted RMSE (lowest value) and RMSE (lowest value). Note that zero weight is lower than 0.7.

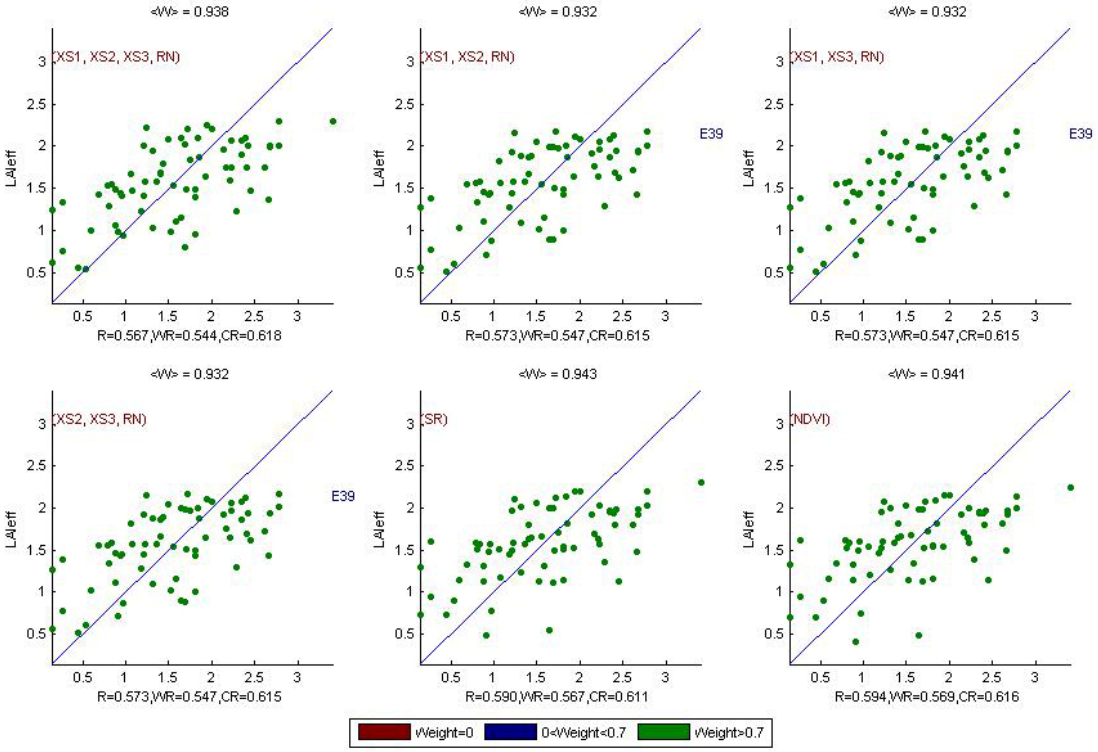

Figure 10. Effective Leaf Area Index: results for regression on reflectance using different band combinations. R is the root mean square error computed between LAIeff and estimated LAIeff. WR is the weighted root mean square error and CR is the cross validation root mean square error.

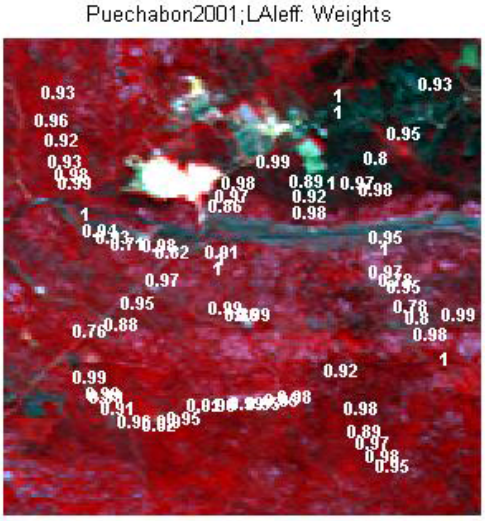

Figure 11. Weights associated to each ESU for the determination of LAIeff transfer function.

For the LAItrue, the XS1, XS2, XS3, RN combination on reflectance (Figure 12 and Figure 13) was selected since it provides the best results: cross-validation RMSE (lowest value), weighted RMSE (lowest value) and RMSE (lowest value). Note that two weights are lower than 0.7.

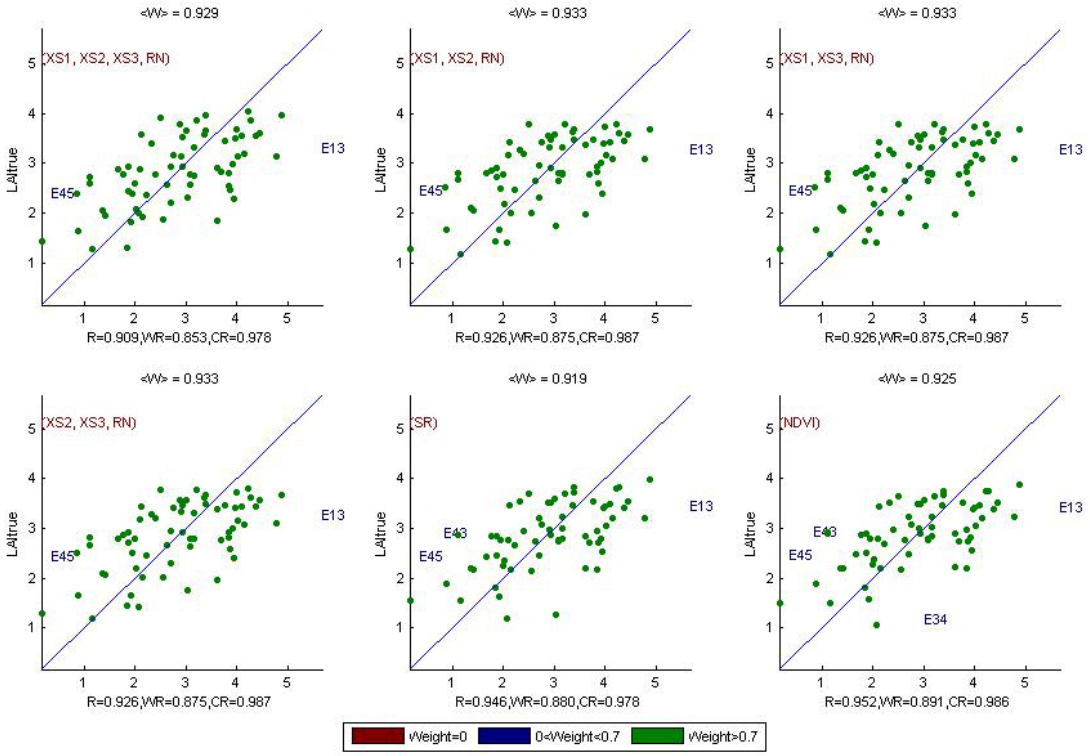

Figure 12. True Leaf Area Index: results for regression on reflectance using different band combinations. R is the root mean square error computed between LAItrue and estimated LAItrue. WR is the weighted root mean square error and CR is the cross validation root mean square error.

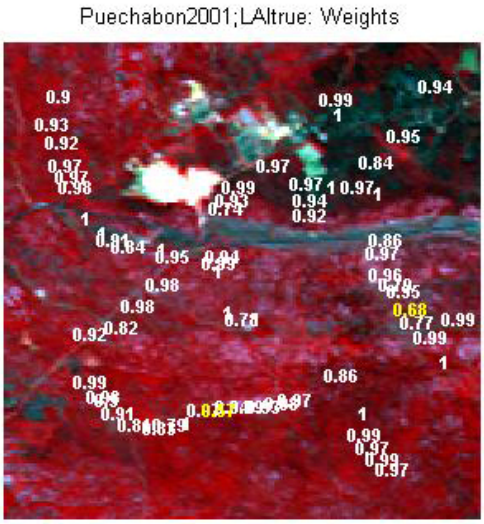

Figure 13. Weights associated to each ESU for the determination of LAItrue transfer function.

For the LAI57eff, the XS1, XS2, XS3, RN combination on reflectance (Figure 14 and Figure 15) was selected since it provides a good compromise between the cross-validation RMSE, the weighted RMSE (lowest value) and the RMSE (lowest value). Note that zero weight is lower than 0.7.

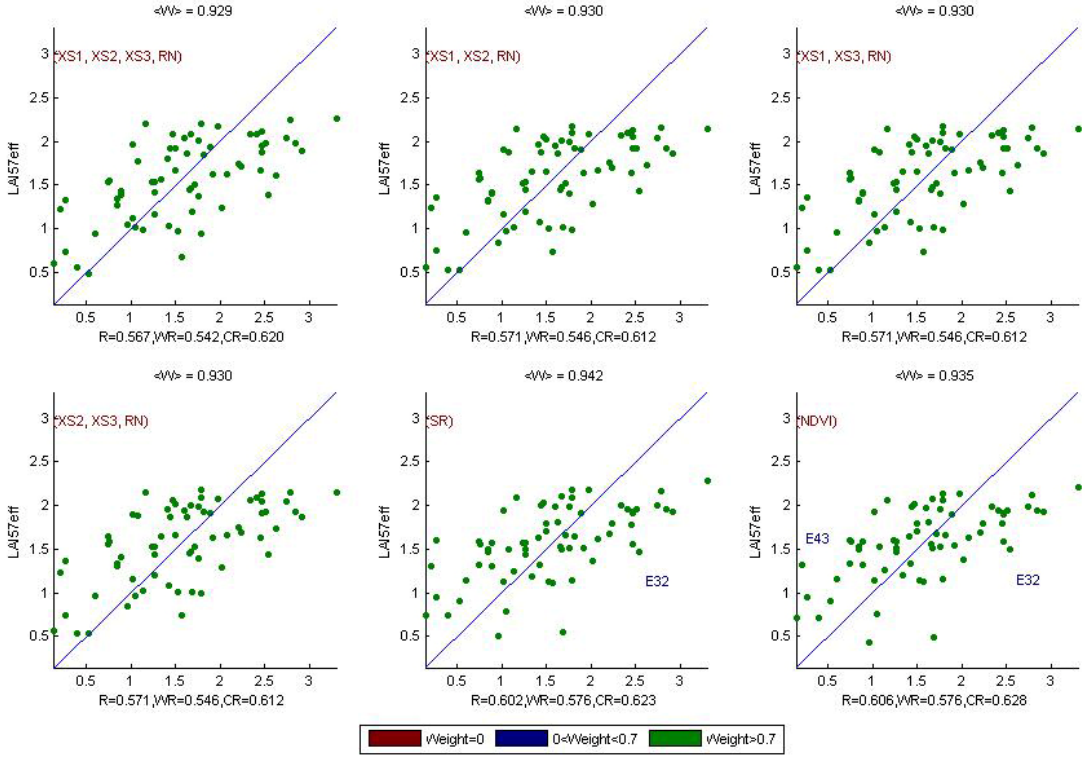

Figure 14. Effective LAI at 57.5°: results for regression on reflectance using different band combinations. R is the root mean square error computed between LAI57eff and estimated LAI57eff. WR is the weighted root mean square error and CR is the cross validation root mean square error.

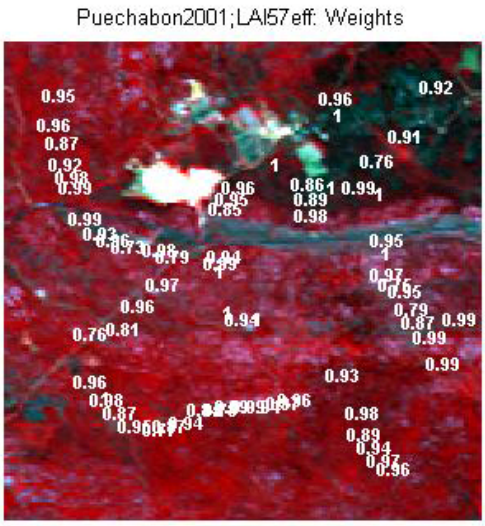

Figure 15. Weights associated to each ESU for the determination of LAI57eff transfer function.

For the LAI57true, the XS1, XS2, XS3, RN combination on reflectance (Figure 16 and Figure 17) was selected since it provides good results: weighted RMSE (lowest value) and RMSE (lowest value). Note that one weight is lower than 0.7.

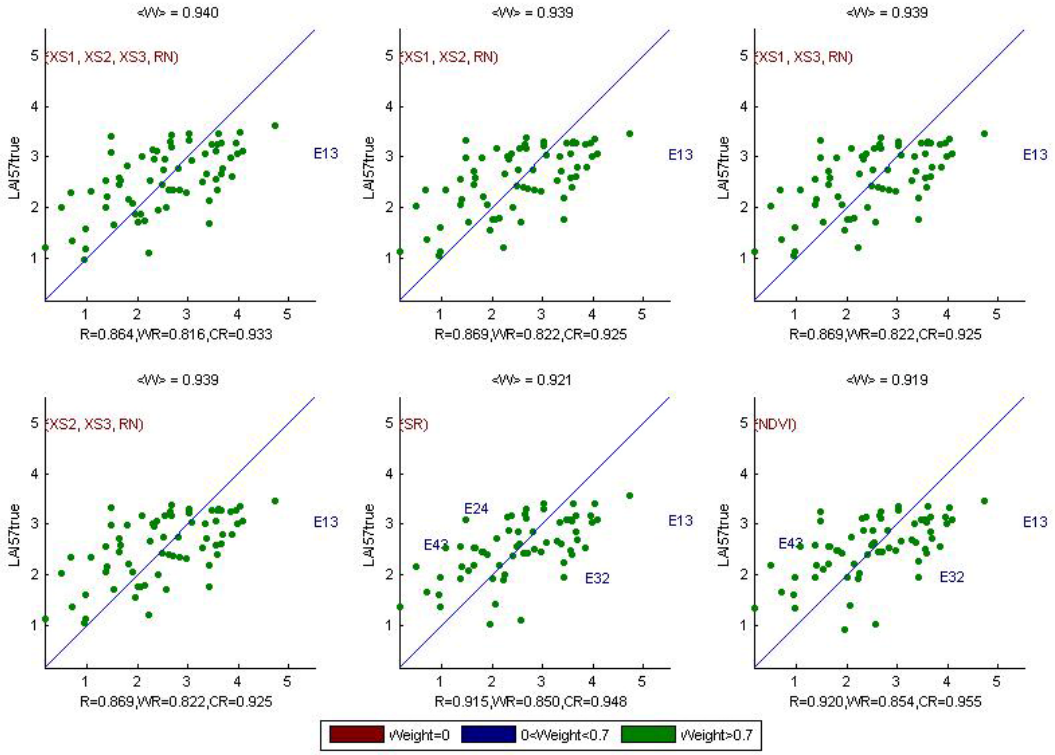

Figure 16. True Leaf Area Index at 57.5°: results for regression on reflectance using different band combinations. R is the root mean square error computed between LAI57true and estimated LAI57true. WR is the weighted root mean square error and CR is the cross validation root mean square error.

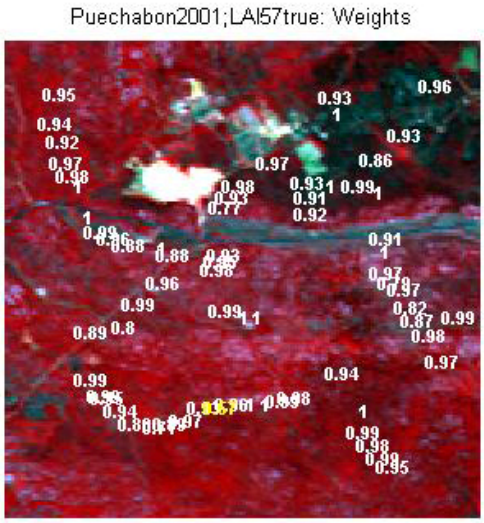

Figure 17. Weights associated to each ESU for the determination of LAI57true transfer function.

For the fCover, the NDVI combination on reflectance (Figure 18 and Figure 19) was selected since it provides good results: weighted RMSE (lowest value) and RMSE (lowest value). Note that three weights are lower than 0.7.

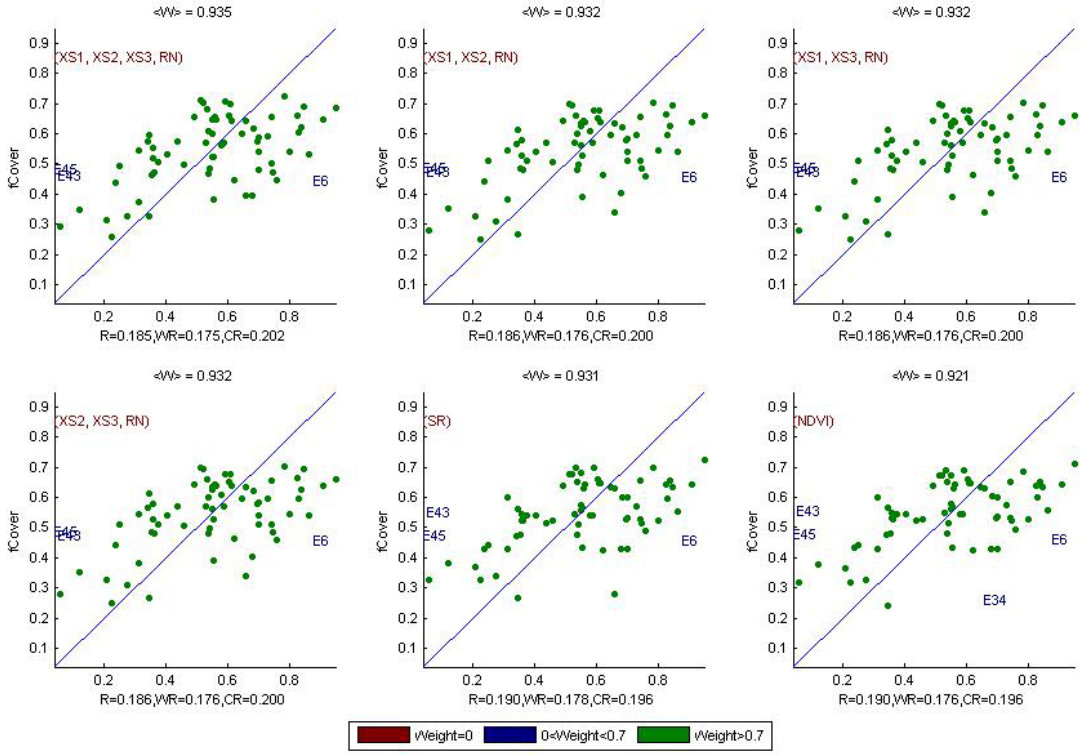

Figure 18. fCover: results for regression on reflectance using different band combinations. R is the root mean square error computed between fCover and estimated fCover. WR is the weighted root mean square error and CR is the cross validation root mean square error.

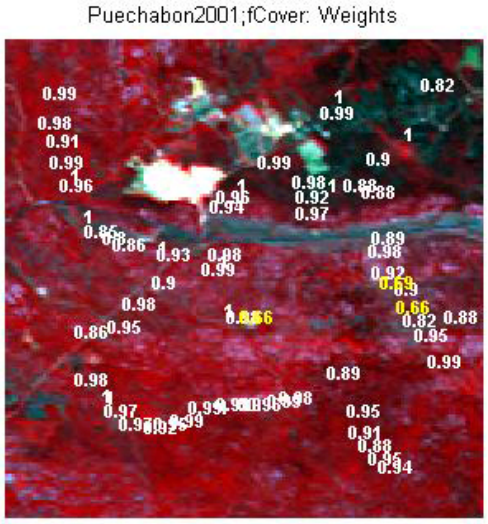

Figure 19. Weights associated to each ESU for the determination of fCover transfer function.

For the fAPAR, the XS2, XS3, RN combination on reflectance (Figure 20 and Figure 21) was selected since it provides a good compromise between the cross-validation RMSE, the weighted RMSE (lowest value) and the RMSE. Note that one weight is lower than 0.7.

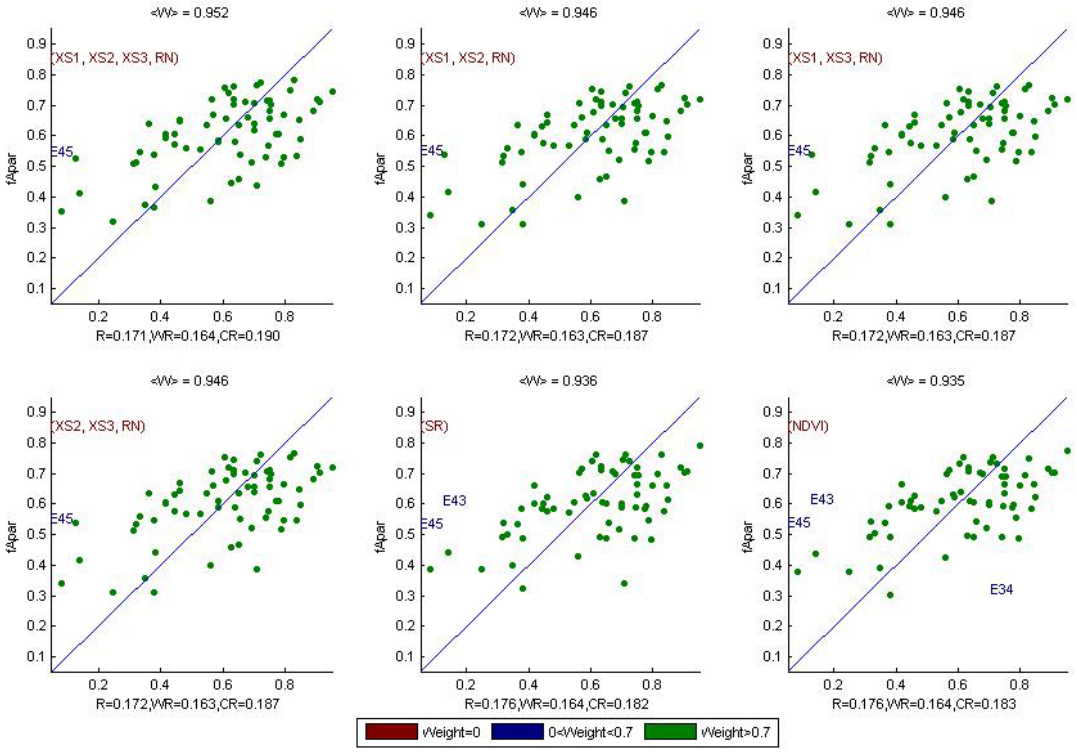

Figure 20. fAPAR: results for regression on reflectance using different band combinations. R is the root mean square error computed between fAPAR and estimated fAPAR. WR is the weighted root mean square error and CR is the cross validation root mean square error.

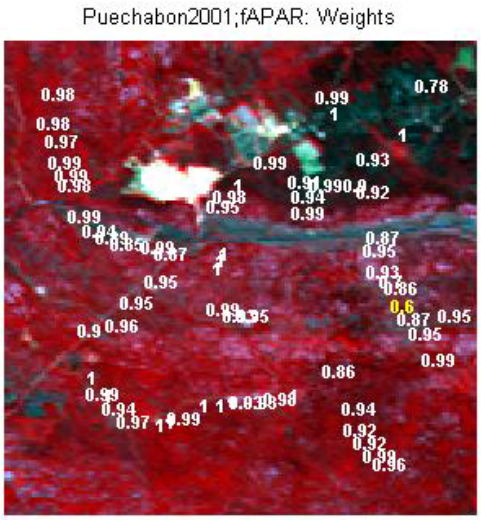

Figure 21. Weights associated to each ESU for the determination of fAPAR transfer function.

Following, the results of the transfer function (Table 2):

Variable	Band Combination	RMSE	Weighted RMSE	CR RMSE
LAIeff	-4.8431 + 20.6353(XS1) + 42.4981(XS2) + 26.4184(XS3) - 291.5417(RN)	0.567	0.544	0.618
LAItrue	-13.0272 + 51.7407(XS1) + 100.5871(XS2) + 56.123(XS3) - 607.6663(RN)	0.909	0.853	0.978
LAI57eff	-2.482 + 13.7429(XS1) + 32.5118(XS2) + 20.3066(XS3) - 246.3015(RN)	0.567	0.542	0.620
LAI57true	-2.7801 + 3.3405(XS1) + 59.4416(XS2) + 30.9996(XS3) - 359.4252(RN)	0.864	0.816	0.933
fCover	-1.1239 + 11.2753(XS1) + 2.5875(XS2) + 5.3202(XS3) - 57.6366(RN)	0.185	0.175	0.202
fAPAR	0.5411 + 10.4409(XS2) -13.8222(XS3) + 0.808(RN)	0.172	0.163	0.187

RN = Red*NIR

Table 2. Transfer function applied to the whole site for the different biophysical variables, and corresponding errors

3.3. Applying the transfer function to the Puéchabon SPOT image extraction

Figure 22 presents the biophysical variable maps obtained with the transfer function described in Table 2 for the classes 1, 2 and 4 (class 3: LAI = 0; please read §3.1). The maps obtained for the six variables are consistent, showing similar patterns: low LAIeff values where low fCover or fAPAR are observed and conversely… The difference between effective LAI and true LAI is significant (see the average values in

Figure 22). This was expected when looking the LAIeff/LAItrue relationship, showing that for high LAI the difference between the two can be significant.

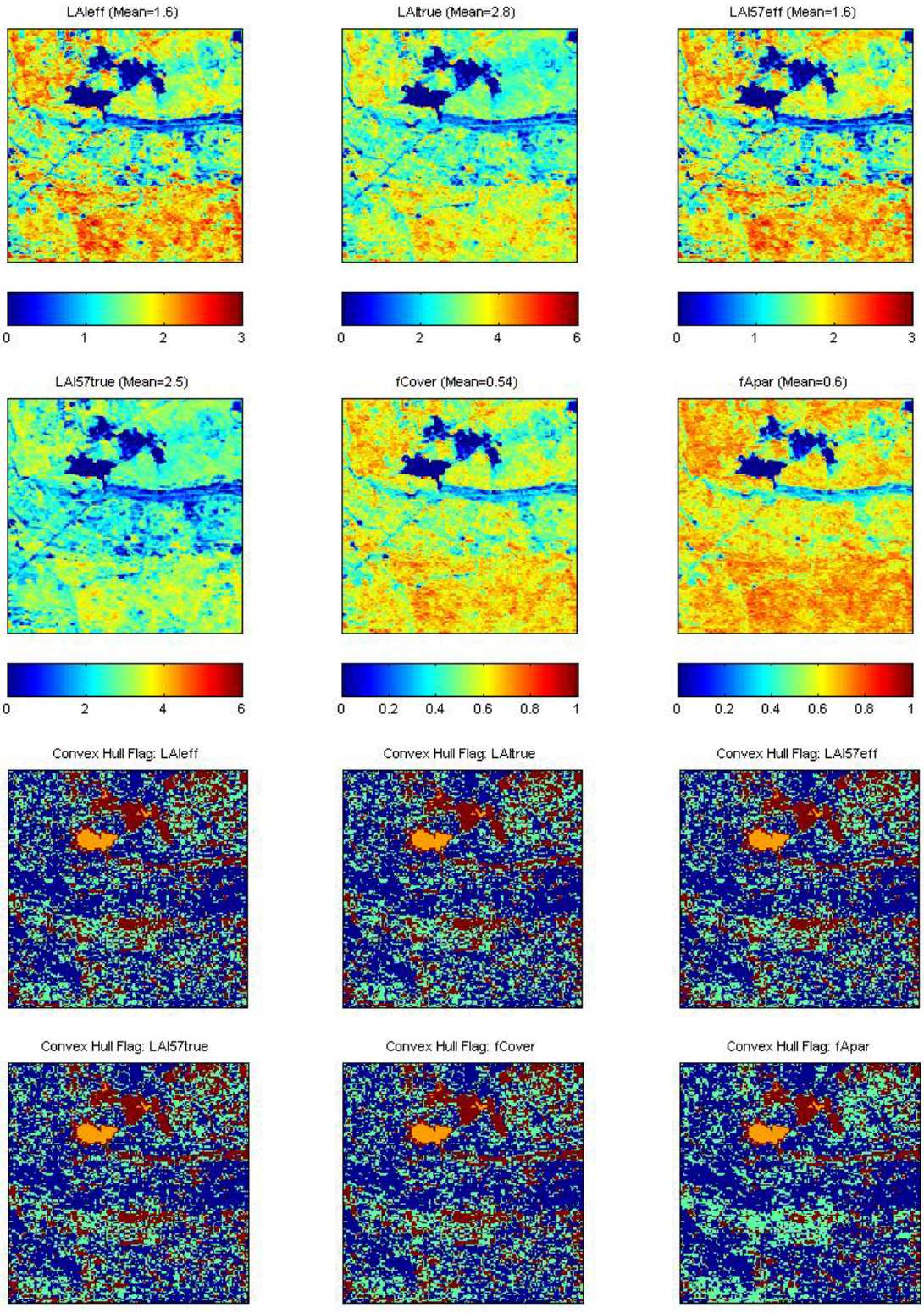

Figure 22. High resolution biophysical variable maps applied on the Puéchabon site (top). Associated flags are shown: blue and light blue correspond to the pixels belonging to the 'strict' and 'large' convex hulls, red to the pixels for which the transfer function is extrapolating and orange to the pixels for which the value 0 is attributed.

The flag maps are comparable. The extrapolation mainly corresponds to bare soil, rocks, lowest NDVI values (§2.3.2). The orange pixels mainly correspond to a quarry (§2.3.3).

4. Conclusion

The 'REG' method is applied to the classes 1, 2 and 4 by using 68 ESUs, whereas the value 0 is attributed to class 3 which mainly corresponds to a quarry (bare soil). The relationship between NDVI and LAI variables is consistent and the representativeness of the land cover of the different ESUs is very good. The results of the robust regression are satisfactory and the maps obtained for the biophysical variables are consistent. The flag associated to each map show that the little extrapolation of the transfer function is mainly bounded to bare soil, rocks (§2.3.2)… For all the variables, the regression coefficients are computed by relating the variable itself to reflectance.

The biophysical variable maps are available in UTM, 31 North, projection coordinates (Datum: WGS-84) at 20 m resolution.

5. Acknowledgements

We thank people who participated to the field experiment: **Marie Weiss** (NOVELTIS, based at INRA), **Bruno Combal**, **Nadine Bruguier**, **Jean-François Hanocq** (INRA), **Roland Bosseno** (IRD, based at INRA), **Hervé Bohbot**, **S. Rambal**, **A. Rochetaud** (CEFE, Montpellier), **Sébastien Garrigues** (CNRM, Toulouse), **Camille Lelong** (CIRAD, Montpellier), **Fabien Dauriac** (CEMAGREF, Montpellier), **Yuri Knyazikhin**, **Grace Smith**, **Jennifer Flax** (Boston University, USA), **Jiarui Dong, Jianan Hu** (Boston University, USA) and **Oleg Panferov** (Institute of Bioclimatology, Göttingen, Germany), but also **Benjamin Baret** (INRA) who processed hemispherical images**.**

ANNEX

VALERI / MODLAND 2001
JOINT CAMPAIGN IN PUĔCHABON (FRANCE)

June 11 – June 15, 2001

Participants:

Marie Weiss - NOVELTIS based at INRA CSE Avignon
Bruno Combal, Nadine Bruguier, Jean-François Hanocq - INRA CSE, Avignon
Roland Bosseno - IRD, based at INRA CSE, Avignon)
Hervé Bohbot, S. Rambal, A. Rochetaud - CEFE, Montpellier
Sébastien Garrigues - CNRM, Toulouse
Camille Lelong - CIRAD, Montpellier
Fabien Dauriac - CEMAGREF, Montpellier

Yuri Knyazikhin, Grace Smith, Jennifer Flax (Boston University, USA)
Jiarui Dong, Jianan Hu (Boston University, USA)
Oleg Panferov (Institute of Bioclimatology, Göttingen, Germany)

A. Introduction

This 1 week campaign is the result of a joint effort from MODLAND and VALERI teams. Puéchabon is located in the South East of France, near Montpellier (Table 1). The site is a 3km by 3km Mediterranean forest mainly composed of oak, box trees, and thyme. It is located near the flux tower of the MELODY[2] project from which many information have already been gathered by the CEFE (S. Rambal's team) since June 1998. Figure 1 is a map of dominant species over the site from 1971. The landscape has not really changed since this date except for the thyme band in the center of the site which is now grassland.

WGS-84	Latitude Longitude	UTM, zone 31
Upper Left	43°44'17" N 03°38'00" E	4843000km N 551000km E
Lower Right	43°42'39" N 03°40'13" E	4840000km N 554000km E

Table 3: Puéchabon VALERI site location.

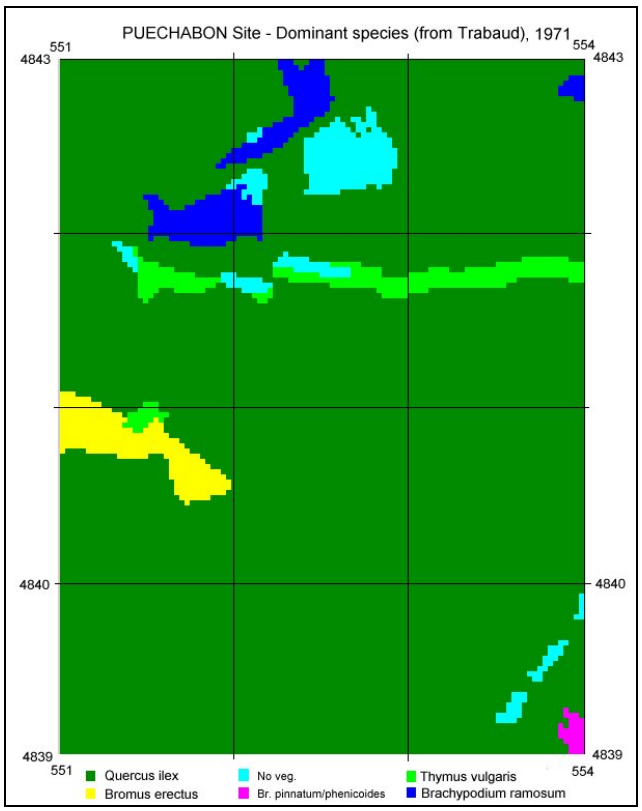

Figure 23. Dominant species of the Puéchabon Site (from Trabaud, 1971).

B. Sampling Strategy and measurement protocol

The objectives of both MODLAND and VALERI projects are to provide LAI[3] and fAPAR[4] at low spatial resolution for large swath satellite product validation. Previous studies on VALERI 2000 campaigns ((De Beaufort, 2000),(Weiss et al., 2000)) based on kriging techniques to interpolate local measurements to the whole site area, have shown that a big effort of sampling is needed. Results have shown that applying collocated kriging between local measurements and variables derived from high spatial resolution images (20m) was the only way to get consistent evaluation of LAI at 1km scale. This method require:

[2] MEditerranean Landscapes in a changing wOrld: coupling Dynamic and functional analyses (http://melody.cefe.cnrs-mop.fr/)
[3] Leaf Area Index
[4] fraction of Absorbed Photosynthetically Active Radiation

1. Footprints of local measurements and high spatial resolution image (SPOT) must be of the same order to calibrate the relationship between SPOT reflectances and measured biophysical variables: each local measurement consists therefore of 4 instrument acquisitions taken every 4m along a 20m long transect (Figure 2). A local measurement thus corresponds to o 4*6 instrument acquisitions.

Figure 24. Sampling strategy for local measurements. The transect is 20m long, four acquisitions (here, hemispherical photographs) are performed at each point which are distant from 4m.

2. On one hand, kriging techniques require variogram (and co-variogram) modeling, *e.g.*, distance levels between local measurements must be well distributed between 0 and 3km. On the other hand, it was not always easy to penetrate inside the canopy, due to bush and very dense forest places. Measurements were therefore performed along existing paths in the forest: every 80m-100m along the path, operators walked 40m inside the canopy to make the 20m transect described here above. Figure 3 presents the whole sampling performed on the Puéchabon site.

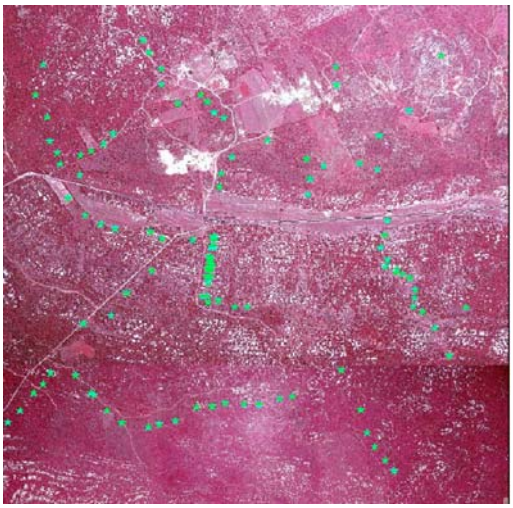

Figure 25. Puéchabon site sampling. Each star corresponds to a 20m transect described in figure2 (Aerial picture IFN, 1992/07/15)

C. Measurements

C.1. Canopy structure variables.

Three instruments were used to evaluate canopy biophysical variables (gap fraction, LAI, and fAPAR):

1. ACCUPAR[5] is a linear PAR ceptometer consisting of an integrated probe that contains 80 PAR photodiodes and a microcontroller. Reference measurements in open areas were acquired before each local measurements (Figure 2). For each of the 24 local measurement acquisitions, PAR radiation acquisition consisted of 5 averaged acquisitions by looking downward, and 5 other by looking upward, instrument being placed at the waste height. ACCUPAR instruments was used during the day to get direct solar radiation.
   During the campaign, two ACCUPAR (BU and CE) were used. Calibration files corresponding to measurements acquired at the same time and the same place, for these instruments, are available.

2. NIKON Coolpix 990, with a fisheye lens FC???? allowed to take hemispherical pictures of the canopy. They were acquired both at the same place and time as the ACCUPAR measurements. Except in open areas where pictures were acquired from above the canopy (short vegetation), the camera was place on the ground, looking upward.
   Several measurements were also performed in diffuse conditions at the same place as LAI2000 to make comparisons between the instruments.

3. LAI2000 were used in diffuse conditions (early in the morning and late in the evening). As the vegetation was quite high, one LAI2000 (sensor #0737) was placed as a reference in an open area (near the house) 5km far from the site. Measurements consist of 8 below acquisitions in open areas. In forest areas, 4 acquisitions were performed at the ground level(figure 2) and 4 at the same place but at understory level. Two instruments were used calibration files between them and the reference are given.

C.2. Leaf and canopy optical properties

Using the Li-18000[6] and ASD[7] instruments, Measurements were collected on June, 12th and 13th at the top of the MELODY tower to measure incident radiation and radiation reflected at the top of the canopy. Measurements were also acquired et ground level to measure canopy spectral transmittance and ground reflectance. On June 13th, 10 leaves, divided in 5 subgroups (sun, shaded, current year, 1 year old, older than 1 year) have also been cut and their spectral properties were measured 2 hours later in the laboratory. The two Li-1800, as well as the ASD were calibrated by taking a series of simultaneous measurements of spectral variation of downward radiation flux densities at the top of the tower.

On June, 14th, spectral up- and downward radiation fluxes (ASD) were measured at each point where ACCUPAR and hemispherical photographs were taken. Two Li-18000 were left in an open area (40m by 40m) to measure spatial and spectral variation of downward radiation fluxes.

C.3. Incoming Radiation fluxes

From June 11th to June 15th, LI1400[8] data logger were programmed to record downward PAR ($mmolm^{-2}s^{-1}$) and SWR (Wm^{-2}) fluxes every second from 5am to 10am. At the same time, a BF2 device[9] acquired downward PAR ($mmolm^{-2}s^{-1}$). Those instruments were all located near the house, at the same place as the LAI2000 reference instrument.

D. References

De Beaufort, L., 2000. Définition d'une méthode de cartographie d'indice foliaire destinée à la validation de produits de capteurs satellites, ENSAR, Rennes.

Weiss, M. et al., 2000. Mapping leaf area index measurements at different scales for the validation of large swath satellite sensors: first results of the VALERI project. In: CNES (Editor), 8th International Symposium in Physical Measurements and Remote Sensing, Aussois, France, pp. 125-130.

[5] http://www.decagon.com/accupar/
[6] http://env.licor.com/products/li1800/1800.htm
[7] http://www.asdi.com/
[8] http://env.licor.com/products/li1400/1400.htm
[9] http://www.delta-t.co.uk/frame/submenu/bf2.html

E. Measurements description

team	day	month	num	hour	minute	easting(m)	northing(m)	Comments on the vegetation status, condition of acquisitions, etc...
1	11	6	1			552282	4841629	box + oaks
1	11	6	2			552274	4841574	
1	11	6	3			552263	4841511	
1	12	6	11	11	50	552311	4841260	open area + oaks on the border
1	12	6	12			552409	4841224	oaks + box understorey
1	12	6	13	12	40	552488	4841227	open area
1	12	6	14			552320	4841926	grass + oaks
1	12	6	15			552328	4842006	grass + oaks + box
1	12	6	16			552393	4842102	grass + oaks + box
1	12	6	17			552608	4842202	grass
1	13	6	2	16	20	552051	4840556	dense oaks + box
1	13	6	3	17	5	552180	4840636	mid dense oaks + box + grass
1	13	6	4	17	37	552272	4840640	very dense vegetation oaks + box
1	13	6	5			552352	4840662	
1	13	6	6			552849	4841880	open area + oaks on the border
1	13	6	7			552862	4841973	thyme + green oaks (1-2m) + grass
1	13	6	8			552946	4842050	thyme + garrigue
1	13	6	9			552842	4842090	oaks
1	14	6	1	10	30	552466	4840659	rocks + oaks+ box (clouds)
1	14	6	2	11	0	552555	4840653	oaks + box understorey
1	14	6	3	11	20	552678	4840688	box + oaks
1	14	6	4	11	50	552755	4840700	box + oaks
1	14	6	5	13	10	551954	4840536	oaks
1	14	6	6	13	30	551889	4840522	box + oaks
1	14	6	7	13	55	551729	4840545	open area (grass + shrubs)
1	14	6	8	14	20	551637	4840619	open area + box
1	14	6	9	14	40	551563	4840710	oaks + box
1	14	6	10	15	10	551539	4840721	oaks + box
1	14	6	11	15	40	551451	4840827	oaks
1	15	6	1	9	10	553270	4842030	open area (grass + oaks)
1	15	6	2	9	20	553164	4842066	open area (grass + oaks + prickly plants)
1	15	6	3	9	30	553282	4842227	oaks + box
1	15	6	4	9	45	553462	4842372	box + oaks + genevrier + rocks (dense, low)
1	15	6	5	10	5	553655	4842700	low vegetation + rocks + sand
2	11	6	1			552153	4841619	forest
2	11	6	2			551910	4841438	forest + open area
2	11	6	3			551759	4841304	
2	11	6	4			551662	4841172	
2	11	6	5			551496	4841124	dense forest
2	12	6	G			553329	4841730	grass (road border)
2	12	6	H			553313	4841647	open garrigue
2	12	6	J			553329	4841499	open area + trees
2	12	6	L			553389	4841441	oaks
2	12	6	M			553464	4841393	green oaks + open area
2	12	6	N			553495	4841278	dense green oaks
2	13	6	1	10	50	553541	4841197	open area + woody plants (low)
2	13	6	2	11	30	553616	4841102	woody plants (low) + low vegetation
2	13	6	3			553701	4840937	woody trees (high: 4m) in edge of the clearing
2	13	6	4			553805	4841223	green oaks (max. 3m) + box dense
2	13	6	5			553018	4842629	grass + thyme + box + oaks (3-4m)
2	13	6	6			553022	4842524	open area + box
2	13	6	7			553051	4840854	green oak (4m) + box
2	14	6	1	11	30	553370	4840266	box + oaks (dense)
2	14	6	2	12	5	553319	4840329	box + oaks
2	14	6	3	12	35	553253	4840407	box + oaks
2	14	6	4	13	5	553206	4840488	box + oaks
2	14	6	5	13	45	553172	4840621	box + oaks
2	14	6	6	15	50	551970	4841626	box + oaks (mid dense)
2	14	6	7	16	20	551899	4841666	box + oaks (dense)
2	14	6	8	16	50	551689	4841682	open area
2	14	6	9	17	25	551604	4841711	open area
2	14	6	10	17	45	551509	4841763	open area
2	14	6	11	18	20	551407	4841861	vineyards + grass + shrubs
2	15	6	1	9	10	551358	4842061	oaks + genevrier
2	15	6	2	9	38	551340	4842124	oaks + genevrier + box + no grass (dense)
2	15	6	3	9	50	551295	4842192	border of open area
2	15	6	4	10	1	551279	4842336	dense vegetation (oaks + box)
2	15	6	5	10	21	551256	4842641	dense vegetation (oaks + low developed understorey)
2	15	6	6	10	30	551210	4842468	border of open area (oaks + box)

F. CONCLUSION

The VALERI/MODLAND 2001 Puechabon Team
(H.Bohbot, N. Bruguier, F. Dauriac, S. Garrigues, C. Lelong, and A. Rocheteau were not here the day the picture was acquired; S. Rambal was behind the camera!)